Modeling and Aalyzing Electromagnets for Magnetic Suspension Systems

Sang Heon Lee[1,#], Yoon Su Baek[2] and Kwang Suk Jung[3]

1 School of Mechanical Engineering, Andong National University, Andong, South Korea
2 School of Mechanical Engineering, Yonsei University, Seoul, South Korea
3 Department of Mechanical Engineering, Chungju National University, Chungju, South Korea
Corresponding Author / E-mail: shlee@andong.ac.kr; Tel: +82-54-820-5908; Fax: +82-54-820-5167

KEYWORDS : Magnetic bearing, Magnetic suspension, Magnetic circuit, Reluctance, Permeance

Various precision engineering studies have attempted to remove mechanical friction, which causes the performance of a system to deteriorate, from precision positioning devices. Since the classical fluid lubrication method has some disadvantages in clean environments, attention has been focused on magnetic bearings and contact-free systems with their pollution-free characteristics. In this paper, f electromagnets are modeled and analyzed, not only for magnetic bearings but also for contact-free electromagnetic actuators. Three types of electromagnets that are appropriate for various applications were considered using magnetic circuitry theory. The results were experimentally validated.

Manuscript received: January 11, 2006 / Accepted: February 8, 2006

NOMENCLATURE

$\boldsymbol{B}$ = magnetic field density
$\boldsymbol{H}$ = magnetic field intensity
L = inductance
λ = magnetic flux linkage
$\boldsymbol{p}$ = position vector
μ_0, μ_r = permeability of air, relative permeability

subscripts:
g = air gap
m = magnetic material

1. Introduction

he requirements for precision manufacturing technology have become much stricter with high level integration of electrical circuits and the miniaturization of mechanical parts. For example, 90-nanometer technology, which used to be thought of as the highest commercial technology available in the semiconductor manufacturing industry, has recently been superseded by 0.10-micron technology. Current trends in the precision manufacturing industry have focused on special machining methods, such as electrochemical machining and photolithography, as alternatives to classical mechanical machining. Despite enhancements in the actual special machining methods, the performance of these methods is largely dependent on the resolution of the positioning system, such as a precision stage. Hence, various studies have attempted to develop precision positioning systems; these have shown that direct-drive and contact-free systems are the most appropriate designs. [1-3]

Contact-free systems using magnetic forces have been used to produce a magnetic levitation vehicle with magnetic bearings, which eliminate mechanical friction. Jayawant [4] divided magnetic levitation and suspension methods into nine classifications. One of these classifications, electromagnetic suspensions, is the focus of the modeling and analysis described in this paper. The main applications of magnetic suspensions are

- single or multi-degree of freedom suspension systems,
- transportation,
- suspensions for wind tunnels,
- magnetic bearings (linear slider, anti-vibration), and
- electrodynamic suspensions.

This paper proposes various types of electromagnets for multi-degree of freedom suspension systems and magnetic bearings, which are related to precision positioning devices. A methodology is presented for designing precision positioning systems by first identifying the characteristics of the electromagnets according to their shape, and then modeling and analyzing the electromagnetic system. A selection process for electromagnets is presented in Section 2. In Section 3, the magnetic forces of each electromagnet are analyzed using magnetic circuitry theory. The proposed analysis is verified by an experiment in Section 4.

2. Selection of Electromagnets

There are two magnetic field effects that result in the production of mechanical forces. The first is the alignment of flux lines, called the variable reluctance (VR) effect; the other is the interaction between magnetic fields and current-carrying conductors, called the Lorentz force.[4] The first has a high power density due to the adoption

of ferromagnetic materials. Thus, the system can be made from a simple structure. When two ferromagnetic pieces become misaligned, a reluctance force is generated between the pieces in the direction of the short magnetic flux to generate a minimum reluctance. The Lorentz force, however, is proportional to the magnitude of the magnetic field and current. In general, a permanent magnet is used to generate the magnetic field. This requires a high current input since the power density is less than the VR principle. Although a high Lorentz force can be obtained by developing strong permanent magnets (*e.g.*, NdFeB), there are still limitations when applying this principle to systems that require strong constant forces over a wide range of operating conditions due to overheating problems caused by the high current and high resistance of the coil turns. Since the VR principle uses highly permeable ferromagnetic material, strong forces can be generated with low currents and the system is relatively free from overheating problems. But this method has a shortcoming: it only generates attractive forces that are different from the Lorentz force, which is either attractive or repulsive. Therefore, it is difficult to conclude which one of these two methods is best suited for electromagnets. Designers must decide by considering the pros and cons of each principle. Since we focused on the development of precision positioning devices that operate in ultrahigh vacuums, the VR high power density principle, which does not have thermal problems, was adopted.

There are two types of forces that are generated by one pair of magnetic elements (active/passive). The first is a unidirectional magnetic force suitable for the suspension of a maglev train and magnetic bearing. The second is a multidirectional force suitable for suspension and propulsion when guidance and propulsion forces are required simultaneously. Three types of electromagnets are available, as shown in Fig. 1, each generating a different force: Model I generates three-directional forces, Model II generates two-directional forces, and Model III generates one-directional forces. A multi-degree of freedom system can be established by combining theses electromagnets.

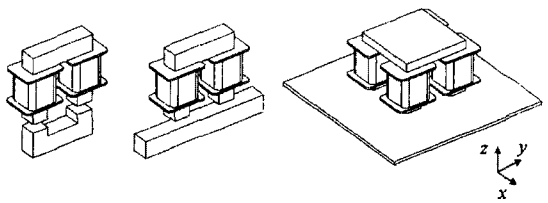

(a) Model I (b) Model II (c) Model III

Fig. 1 Types of electromagnet

3. Modeling the Electromagnets

3.1 Magnetic Circuit

A magnetic field is a distributed parameter phenomenon; *i.e.*, it is distributed over a region of space. As such, a rigorous analysis requires the use of the distance variables contained in the divergence and curl symbols. However, under proper conditions, it is possible to apply a lumped-parameter analysis to certain classes of magnetic field problems just as it is applied in electrical circuit analyses.

This section describes a lumped circuit analysis applied to magnetic systems, often called a magnetic circuit analysis. It is useful for sizing the magnetic components of an electromagnetic device during the design stages, calculating inductances, and determining the air gap flux densities for power and torque calculations. [5,6]

3.2 Magnetic Element

Table 1 shows the relationship between a magnetic circuit and an electric circuit. With recent advances in computer technology, a finite element analysis (FEA) can be used to solve magnetic field

Table 1 Analogy between the magnetic and electric circuits

Magnetic element		Electric element	
MMF	$F = \int \mathbf{H} \cdot d\mathbf{l}$	Voltage	V
Magnetic Flux	$\phi = \int_S \mathbf{B} \cdot d\mathbf{S}$	Current	I
Reluctance	$\Re = \frac{F}{\phi} = \frac{Hl_m}{BA_m} = \frac{l_m}{\mu A_m}$	Resistance	R
Permeance	$\wp = 1/\Re$	Conductance	G
Inductance	$L = \frac{\lambda}{i} = \frac{N\phi}{i}$	Inductance	L
Ampere's circuit law		Kirhihoff's closed equation	

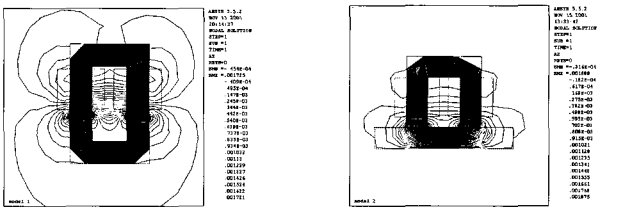

(a) (b)

Fig. 2 Magnetic flux path, leakage flux, and fringing effects obtained using an FEA program (ANSYS 5.5): (a) Model I, (b) Model II

problems, especially multi-physical problems. But this takes a considerable amount of time and is therefore not appropriate for the design stages. The accuracy of magnetic circuit analyses is less than that of electrical circuit analyses due to the relatively small permeability variation between magnetic conductors and insulators and the phenomenon of fringing and leakage fluxes at the end of poles. But its accuracy and precision can be enhanced by precise modeling of the fringing and leakage fluxes. Fig. 2 shows the magnetic flux path in an electromagnet, the leakage flux in an iron-core solenoid, and the fringing effect in the air gap. The fringing and leakage fluxes are modeled geometrically in Fig. 3(a) for each electromagnet, obtaining the equivalent magnetic circuit shown in Fig. 3(b). Assuming that the leakage flux is small enough to be ignored, the magnetic force is derived by modeling the fringing and leakage fluxes as shown in Fig. 3(a) and using a permeance model in the air gap and magnetic elements as shown in Fig 3(b). The same magnetic circuits but different permeance models were used for Models I and II. The expanded magnetic circuit shown in Fig. 3(b) was used for Model III.

The governing equation of the magnetic circuit can be derived using Ampere's law in integral form to describe the magnetic field in the material.[7] Ampere's law is

$$\oint \mathbf{H} \cdot d\mathbf{L} = I_f , \tag{1}$$

where I_f is the current linking the closed path of the integration. The left-hand term in Equation (1) can be expressed by the definition of a magnetic element:

$$\oint \mathbf{H} \cdot d\mathbf{L} = H_m l_m + H_g l_g = \phi(\Re_m + \Re_g) = \Im_m + \Im_g . \tag{2}$$

Since the right-hand term in Equation (1) is the current linking the closed path of integration, it can be expressed by the summation of products of the number of coil turns and the current input,

$$I_f = \sum_{n=1}^{2} N_n i_n , \tag{3}$$

where N and i are the coil turns and current, respectively. By

substituting Equations (2) and (3) into Equation (1), the governing equation for the magnetic circuit becomes

$$\mathfrak{F}_m + \mathfrak{F}_g - \sum_{n=1}^{2} N_n i_n = 0 \cdot \tag{4}$$

This equation indicates that the summation of the magnetic potential in a closed magnetic loop is zero, which is equivalent to Kirchhoff's closed equation in an electric circuit.

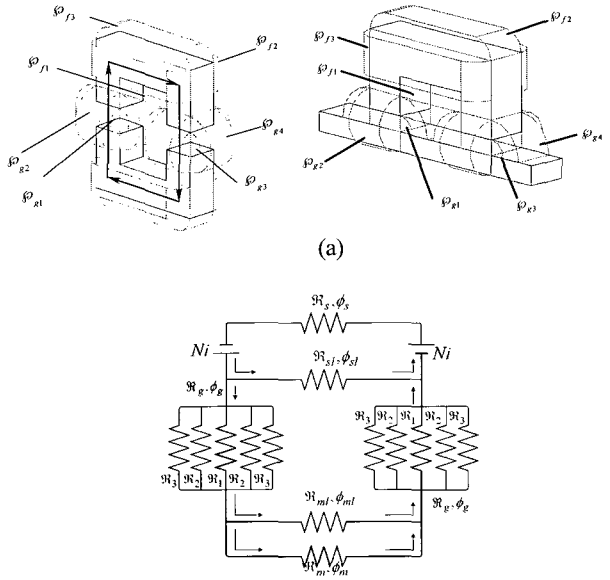

Fig. 3 (a) Flux patterns in electromagnet Models I and II; (b) equivalent magnetic circuit

3.3 Permeance Model

The magnetic flux at the point of interest can be calculated from Equation (1). However, more consideration must be given to the fringing and leak fluxes in the air gap to obtain an accurate result. Hence, a precise permeance or reluctance model is presented in this section. Although the FEA gives a magnetic flux pattern, it is the geometrically driven flux pattern shown in Fig. 4 that is used to obtain an analytical solution. Since the pole shape is the main parameter that determines the magnetic force, two force equations are derived according to the pole shape. This effect will be discussed later. Fig. 4 shows the flux patterns of the rectangular/rectangular poles and wedged/rectangular poles. The reluctance in the air gap was modeled using a serial connection to the flux patterns. The reluctance of each pattern in Fig. 4(a) was obtained from the following definition:

$$\mathfrak{R}_1 = \frac{z}{\mu_0 (w_t - x) l_t} \tag{5}$$

$$\mathfrak{R}_2 = \frac{1}{0.54 \mu_0 l_t} \tag{6}$$

$$\mathfrak{R}_3 = \frac{\pi}{2\mu_0 l_t \log_e (1 + \frac{2x}{z})}, \tag{7}$$

where w_t and l_t are the width and length of the pole. The reluctance in the air gap is

$$\mathfrak{R}_g = \frac{\mathfrak{R}_1 \mathfrak{R}_2 \mathfrak{R}_3}{\mathfrak{R}_2 \mathfrak{R}_3 + 2\mathfrak{R}_3 \mathfrak{R}_1 + 2\mathfrak{R}_1 \mathfrak{R}_2} \cdot \tag{8}$$

The reluctance in the air gap shown in Fig. 4(b) was derived using the same process (see the appendix for details):

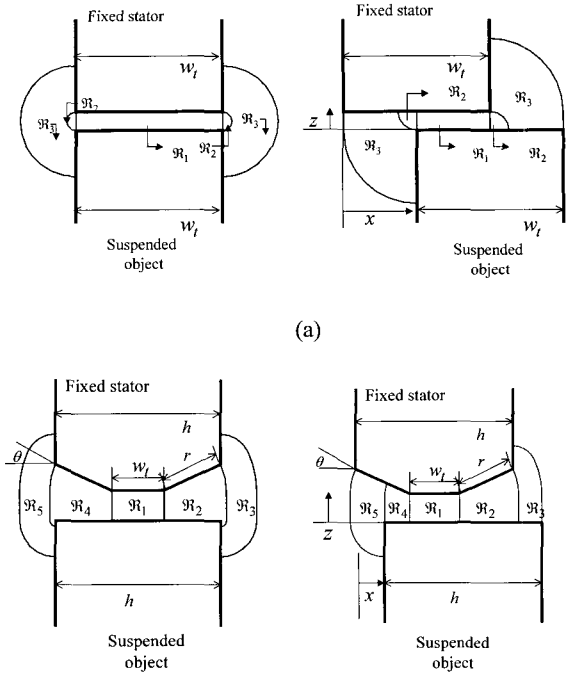

Fig. 4 Flux pattern model: (a) rectangular/rectangular poles; (b) wedged/rectangular poles

$$\mathfrak{R}_g = \left(\frac{\mathfrak{R}_2 \mathfrak{R}_3 \mathfrak{R}_4 \mathfrak{R}_5 + \mathfrak{R}_1 \mathfrak{R}_3 \mathfrak{R}_4 \mathfrak{R}_5 + \mathfrak{R}_1 \mathfrak{R}_2 \mathfrak{R}_4 \mathfrak{R}_5}{\mathfrak{R}_1 \mathfrak{R}_2 \mathfrak{R}_3 \mathfrak{R}_4 \mathfrak{R}_5} + \frac{\mathfrak{R}_1 \mathfrak{R}_2 \mathfrak{R}_3 \mathfrak{R}_5 + \mathfrak{R}_1 \mathfrak{R}_2 \mathfrak{R}_3 \mathfrak{R}_4}{\mathfrak{R}_1 \mathfrak{R}_2 \mathfrak{R}_3 \mathfrak{R}_4 \mathfrak{R}_5} \right)^{-1}. \tag{9}$$

The reluctance in the iron core is

$$\mathfrak{R}_m = \frac{l_m}{\mu_r w_t l_t}, \tag{10}$$

where l_m is the length of the flux path in the iron core. From Equations (5), (6), and (10), the reluctance is related to the length and cross-sectional area of the flux path. The relative permeability of iron is high enough to ignore the reluctance of iron so that Equation (4) becomes a function of the magneto-motive force and current. The leakage flux also has little effect on the entire system so that the magnetic flux in the air gap can be simplified to

$$\phi_g = \mathfrak{R}_g^{-1} \sum_{n=1}^{2} N_n i_n = \wp_g \sum_{n=1}^{2} N_n i_n \cdot \tag{11}$$

3.4 Magnetic Force

Energy conversion is possible due to the interchange between the electrical and mechanical energies through the coupling fields. This leads to a method for determining the mechanical forces that arise from changes in the stored magnetic energy. [6] The conservation of energy can be expressed as

$$Fdx + vidt = dW_m, \tag{12}$$

where Fdx, $vi\,dt$, and dW_m are the mean mechanical energy, electrical energy, and magnetic energy increase in the stored energy, respectively. Neglecting the saturation of the magnetic element, the stored magnetic energy can be written as

$$W_m = \frac{1}{2}Li^2 = \frac{1}{2}\lambda i \,. \tag{13}$$

The magnetic energy and coenergy are the same for a linear magnetic circuit. Following the same procedure that was used to derive the force equations, the force equation can be expressed in terms of the coenergy as [6]

$$\mathbf{F} = \frac{\partial W_m{}'}{\partial \mathbf{p}}(i, \mathbf{p}) \,. \tag{14}$$

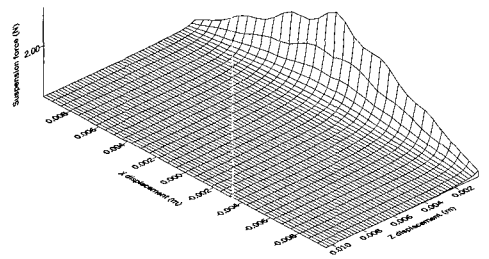

(a)

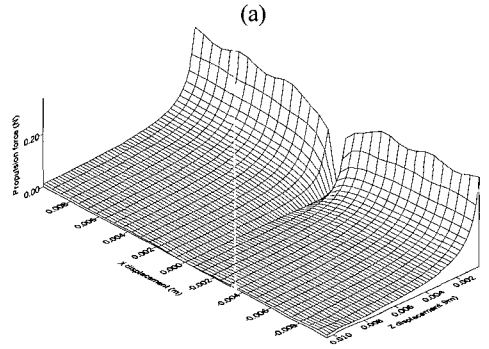

(b)

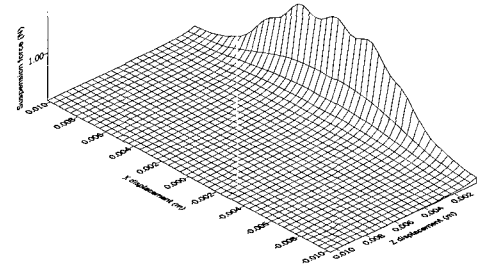

(c)

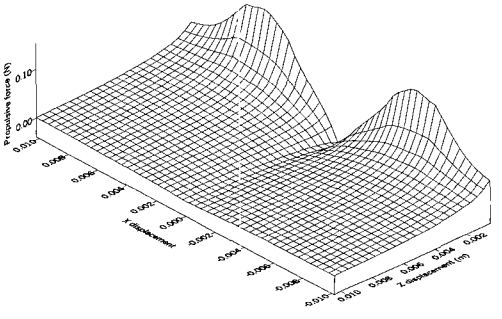

(d)

Fig. 5 Simulation results: (a) and (b) are the vertical and horizontal orces for rectangular/rectangular poles, and (c) and (d) are the vertical and horizontal forces for wedged/rectangular poles

From Equation (13), which describes the stored magnetic energy, it can be deduced that the inductance L is $N^2 \wp_g$ and the magnetic force is dependent on the gradient of the air gap permeance. The gradient of the permeance in the z direction is the same for all the electromagnets described in Section 2, but the permeance in the x or y direction is zero for Models II and III so that there is no magnetic force in those directions.

The calculated magnetic forces are shown in Fig. 5: (a) and (b) give the results for rectangular/rectangular poles while (c) and (d) give the results for wedged/rectangular poles. Electromagnet Model I had the same magnetic forces in the x and y directions. From Fig. 5, it is evident that the air gap is the main parameter that determines the magnitude of the vertical and horizontal forces. Hence, controlling the air gap size is the key technology for stabilizing magnetic suspension systems. The force ratio (fx/fz) of the wedged/rectangular poles (Fig. 5(c) and (d)) was greater than that of the rectangular/rectangular poles (Fig. 5(a) and (b)). Thus, the wedged/rectangular poles benefit design systems that require high propulsion forces for the same vertical force. Similar results were obtained from the experiment described in the next section. Since the shapes of the poles determine the characteristics of the generated forces, the pole shape must be designed according the ultimate purpose of the system.

4. Experimental Verification and Discussion

Experiments were performed to verify the equations derived in the previous section. The vertical and horizontal magnetic forces were measured using a force/torque sensor (ATI, FT3940) that measured forces and torques with 0.05 N and 0.003 Nm resolution for six degrees of freedom while the air gap was varied using a constant input current. The stiffness of the sensor was sufficiently high to assume a rigid body. Other mechanical parts in the experimental setup were designed to have a high stiffness to maintain the air gap constant independent of the magnitude of the magnetic force. The experimental setup is shown in Fig. 6, and the specifications of the electromagnet defined in Fig. 4 and used for these tests are given in Table 2. The width of the wedge pole was 4 mm and the wedge angle was 15°. The core material was SS-41, which has a carbon content below 0.23%. In general, carbon enhances the mechanical performance of iron and deteriorates its magnetic performance; the designer must choose an appropriate carbon content for a given application. [8] Laminated silicon steel has good magnetic properties and is easy to obtain, but it is usually available only in standard sizes. Thus, there are limited choices for the designed pole shape when laminated silicon steel is used. The bobbin used for the coil winding is also standardized; therefore, the bobbin and electromagnet should be designed simultaneously. A standard bobbin and electromagnet with 10 × 10-mm cross sections were used for these tests.

Fig. 7 shows the experimental results obtained using rectangular/rectangular poles with an input current of 0.45 A. The discrepancies between the theoretical and experimental values were small, both in terms of quantity and quality. However, the

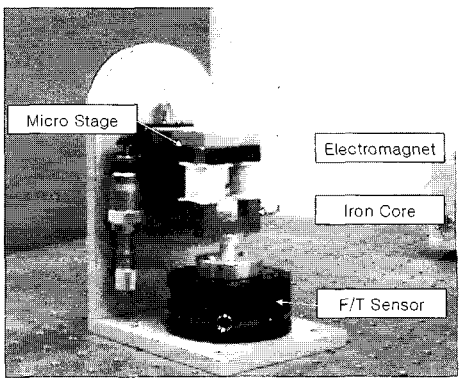

Fig. 6 Experimental setup

Table 2 Dimensions of the electromagnet

Experimental condition	
Coil turns	335 turns
Pole width	10mm
Pole length	10mm
core material	SS-41
Wedge angle	15°
Wedge end width	4mm

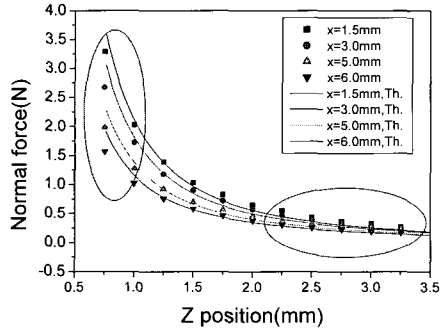

(a)

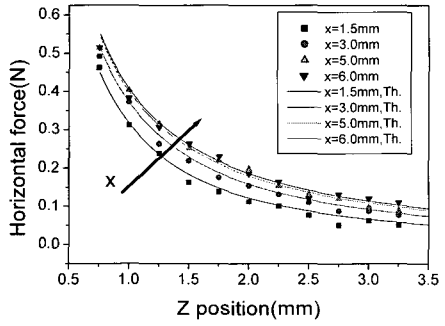

(b)

Fig. 7 Comparison of theoretical and experimental results for rectangular/rectangular poles: (a) vertical force, (b) horizontal force

discrepancies for the vertical or suspension force increased as the air gap (z) decreased, as shown in Fig. 7(a). These forces were too small and a high input current was required to obtain a sufficient suspension force. However, a high input current can cause magnetic saturation, resulting in a deterioration of the magnetic properties of the material. It is therefore recommended to avoid nominal gaps that fall within circles shown in Fig. 7(a). The gradient of the vertical force is negative in Fig. 7(a), which infers that the suspension system is open-loop unstable and requires closed-loop control to stabilize the system. The horizontal force shown in Fig. 7(b) became constant as the horizontal displacement (x) increased. Thus, it is possible to obtain a constant horizontal force over a certain range and to generate a constant propulsion force over the entire operating range with the proper allocation of poles.

Fig. 8 shows the results obtained for the wedged/rectangular poles, as well as other combinations of poles. The theoretical force equation was verified using the results shown in Fig. 8(a). Fig. 8(b) illustrates the effects of the pole shape. The force ratio (horizontal/vertical) of the rectangular/rectangular poles was 0.268. By changing the shape of the poles, it was possible to obtain a higher force ratio of 0.465, which is 1.73 times greater. These results indicate that a wedged pole is appropriate for a system that requires a high propulsion force ratio while a rectangle pole is appropriate for a

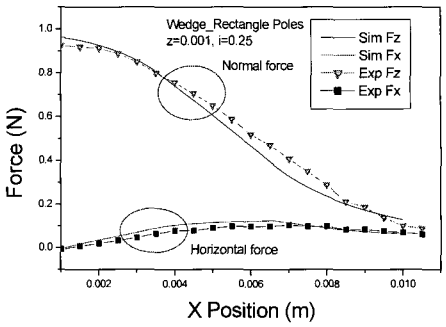

(a)

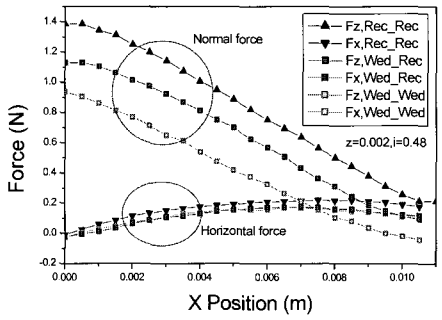

(b)

Fig. 8 Experimental results for various pole shapes: (a) comparison of theoretical and experimental results for wedge/rectangular poles, (b) results obtained for various combinations

system that requires a high suspension force, such as a magnetic bearing.

Fig. 9 shows the measured vertical force of electromagnet Model II with respect to the y direction displacement. A constant vertical force was obtained since the gradient of permeance in the y direction is constant for this electromagnet. However, the characteristics of the forces with respect to other directional displacements were the same as shown in Fig. 7. The vertical force was constant in the x–y plane for electromagnet Model III and no horizontal force existed.

5. Conclusions

This paper presented a modeling and analysis technique for electromagnets used in precision positioning devices, such as multi-degree of freedom suspension systems, magnetic bearings, and contact-free actuators. A design methodology was proposed for three types of electromagnets by modeling and analyzing the Magnetic

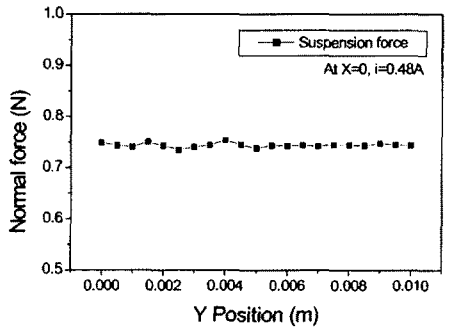

Fig. 9 Vertical force distribution for Model II with respect to the horizontal displacement

effects using magnetic circuit theory. The validity of the modeling and analysis was verified experimentally. It is expected that the modeling and analysis of the electromagnet models proposed in this paper will offer fundamental data and guidelines for developing multi-degree of freedom suspension systems.

REFERENCES

1. Jung, K. S. and Baek, Y. S., "Precision Stage Using a Novel Contact-Free Planar Actuator Based on Combination of Electromagnetic Forces," Trans. of KSME A, Vol. 25, No. 11, pp. 1863-1872, 2001.
2. Jung, K. S., Lee, S. H. and Baek, Y. S., "Feasibility Study of General-purpose Precision Stage Using A Novel Contact-Free Surface Actuator Based on Magnetic Suspension Technology," Trans. Of KSME A, Vol. 26, No. 3, pp. 452-460, 2002.
3. Kim, W. J., Trumper, D. L. and Jeffrey, H. L., "Modeling and Vector Control of Planar Magnetic Levitator," IEEE Trans. on Industry Applications, Vol. 34, No. 6, pp. 1254-1262, 1998.
4. Jayawant, B. V., "Electromagnetic Levitation and Suspension Techniques," London: Edward Arnold, pp. 1-19, 1980.
5. Nasar, S. A. and Unnewwehr, L. E., "Electromechanics and Electric Machines," New York: John Wiley & Sons, Inc., pp. 121-123, 1983.
6. Roters, H. C., "Electromagnetic devices," New York: John Wiley & Sons, Inc., pp. 84-150, 1951.
7. Griffiths, D. J., "Introduction to Electrodynamics," Seoul: Kyo Hak Sa Publishing, pp. 227-250, 1989.
8. Sake, Y. and Hitoshi, Y., "Electromagnetic Levitation System by Means of Salient-Pole Type Magnets Coupled with Laminated Slotless Rails," IEEE Trans. on Vehicular Technology, Vol. 39, No. 1, pp. 83-87, 1990.

APPENDIX

The reluctance models for wedged/rectangular poles with respect to the x directional displacement can be derived as follows. For ($0 \le x < r\cos\theta$),

$$\Re_1 = \frac{z}{\mu_0 l_t w_t}$$

$$\Re_2 = \frac{\theta}{\mu_0 l_t}\log\left(\frac{z+r\theta}{z}\right)^{-1}$$

$$\Re_3 = \frac{\pi}{2\mu_0 l_t}\log\left(\frac{z+(r\cos\theta+x)\theta+(r\cos\theta+x-r)(\pi/2-\theta)}{z+r\theta}\right)^{-1}$$

$$\Re_4 = \frac{\theta}{\mu_0 l_t}\log\left(\frac{z+(r\cos\theta-x)\theta}{z}\right)^{-1}$$

$$\Re_5 = \frac{(\pi/2+\theta)}{\mu_0 l_t}\log\left(\frac{r\theta+z+(r-r\cos\theta+x)(\pi/2)}{z+(r\cos\theta-x)\theta}\right)^{-1}$$

For ($r\cos\theta \le x < w_t$),

$$\Re_1 = \frac{z}{\mu_0 l_t (w_t - x + r\cos\theta)}$$

$$\Re_2 = \frac{\theta}{\mu_0 l_t}\log\left(\frac{z+r\theta}{z}\right)^{-1}$$

$$\Re_3 = \frac{\pi}{2\mu_0 l}\log\left(\frac{z+r\theta+(\pi/2)(l-r-w_t+x-r\cos\theta)}{z+r\theta}\right)^{-1}$$

$$\Re_4 = \frac{\pi}{2\mu_0 l}\log\left(\frac{z+(\pi/2+\theta)(r-r\cos\theta+x)}{z+(r\cos\theta-x)\theta}\right)^{-1}$$

$$\Re_5 = \frac{(\pi/2+\theta)}{\mu_0 l_t}\log\left(\frac{z+r\theta+(r+x-r\cos\theta)\pi/2}{z+(x-r\cos\theta)\pi/2}\right)^{-1}$$

For ($w_t \le x < w_t + r\cos\theta$),

$$\Re_1 = \frac{(\theta+\pi/2)}{\mu_0 l_t}\log\left(\frac{z+(\theta+\pi/2)}{z+\theta(x-w_t-r\cos\theta)}\right)^{-1}$$

$$\Re_2 = \frac{\theta}{\mu_0 l_t}\log\left(\frac{r\theta+z}{z+(x-w_t-r\cos\theta)}\right)^{-1}$$

$$\Re_3 = \frac{\pi}{2\mu_0 l_t}\log\left(\frac{z+r\theta+(\pi/2)(h-r+x-w_t-r\cos\theta)}{z+r\theta}\right)^{-1}$$

$$\Re_4 = \frac{\pi}{2\mu_0 l_t}\log\left(\frac{z+(x-r\cos\theta)\pi/2}{z+(x-w_t-r\cos\theta)\pi/2}\right)^{-1}$$

$$\Re_5 = \frac{(\theta+\pi/2)}{\mu_0 l_t}\log\left(\frac{z+r\theta+(r+x-r\cos\theta)\pi/2}{z+(x-r\cos\theta)\pi/2}\right)^{-1}$$